Biosensors and Bioelectronics 145 (2019) 111611

Contents lists available at ScienceDirect

Biosensors and Bioelectronics

journal homepage: www.elsevier.com/locate/bios

Electrochemical molecularly bioimprinted siloxane biosensor on the basis of core/shell silver nanoparticles/EGFR exon 21 L858R point mutant gene/siloxane film for ultra-sensing of Gemcitabine as a lung cancer chemotherapy medication

Yalda Shoja[a,*], Ahmad Kermanpur[a], Fathallah Karimzadeh[a], Javad Ghodsi[b,**], Amir Abbas Rafati[b], Siavash Adhami[a]

[a] Department of Materials Engineering, Isfahan University of Technology, Isfahan, 84156-83111, Iran
[b] Department of Physical Chemistry, Faculty of Chemistry, Bu-Ali Sina University, P.O.Box 65174, Hamedan, Iran

ARTICLE INFO

Keywords:
DNA biosensor
EGFR exon 21
Molecularly bioimprinted siloxane polymer
Ag NPs
Gemcitabine

ABSTRACT

In search for improvements in bioanalysis electrochemical sensors, for better assessment of anti-cancer drugs, it is necessary for their detection limits to be minimized and the sensitivity and selectivity to be surpassed simultaneously; whereas, resolving any probable interfering with other medical treatments are considered. In this work, a novel approach was adopted for detection and assessment of Gemcitabine (GEM) as an anti-cancer drug based on evaluating its interaction with EGFR exon 21-point mutant gene. An electrochemical nanobiosensor was invented based on a new molecularly bioimprinted siloxane polymer (MBIS) strategy; in which the EGFR exon 21 acts as an identification probe. The roles of multi-walled carbon nanotubes and Ag nanoparticles (NPs) are to perform as a signal amplifier. The MBIS film was prepared by acid-catalysed hydrolysis/condensation of the sample solution, containing Ag NPs, ds-DNA of EGFR exon 21 point mutant gene, GEM as a template molecule, 3-(aminopropyl) trimethoxysilane (APTMS) and tetraethoxysilane. The interaction between the dsDNA and GEM was investigated by employing the modified biosensor and monitoring oxidation signal of guanine and adenine. The produced biosensor was characterized by XRD, FE-SEM, EDS, FT-IR and differential pulse voltammetry. The oxidation signals of adenine and guanine were in linear range when the device was subjected to various concentrations of GEM, from 1.5 to -93 μM, where a low detection limit 12.5 nmol L^{-1}, and 48.8 nmol L^{-1} were recorded by guanine and adenine respectively. The developed biosensor did perform very well when employed for the actual samples; the stability was also approved which was acceptable for a reasonable time.

1. Introduction

Gemcitabine (GEM) is basically a cytosine nucleoside analogue employed for chemotherapy medication (Scheme 1). The ideal role, expected from GEM, is to deal with the solid tumours in different organs of human body e.g. ovary, pancreas, brain, lung, bladder, and breast. Perhaps the most interesting feature of GEM is its compatibility with other anti-cancer drugs; where the treatment procedure can be more effective. In essence, GEM belongs to a category of medicines, which are capable of resembling a normal cell nutrient for the cancer cells; technically, they act as antimetabolites. It is prescribed to be given by an intravenous injection. The metabolism takes a place by liver cytidine deaminase to create inactivated 2′, 2′-di-fluorodeoxyuridine (dFdU) and plasma. The latter is assimilated into DNA, leading to apoptosis (Aydoğdu et al., 2016; Kirstein et al., 2006; Rosell et al., 2003; Shelley et al., 2011). Considering the mentioned points, in order to provide the most effective treatment procedures, the vital issue is the precise dosage determination of GEM in biological and pharmaceutical therapy.

Of course, many analytical methods have been reported so far regarding GEM determination in different cases around the world; along with several methods, including chromatographic techniques e.g. LC/MS/MS (Wickremsinhe et al., 2010; Honeywell et al., 2007), and HPLC

* Corresponding author.
** Corresponding author.
E-mail addresses: yalda.shoja.iut@gmail.com, yalda_shoja1981@yahoo.com, y.shoja@ma.iut.ac.ir (Y. Shoja), ghodsij@gmail.com, j.ghodsi90@basu.ac.ir (J. Ghodsi).

https://doi.org/10.1016/j.bios.2019.111611
Received 18 June 2019; Received in revised form 14 August 2019; Accepted 17 August 2019
Available online 09 September 2019
0956-5663/

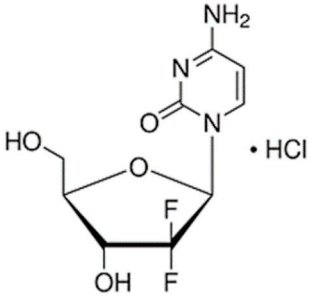

Scheme 1. Chemical structure of gemcitabine.

(Kirstein et al., 2006; Lanz et al., 2007), for assessment of GEM in urine, blood, and tissues. However, despite the advantages of the mentioned methods, they have some disadvantages. They are time consuming procedures, it takes a long time to analyse and interpret the obtained data, in some cases the samples preparation is relatively difficult, the selectivity is quite low, they operate with organic solvents, they are not very economical, etc.

As usual, the science came to help and scientists introduced the advanced biosensing methodologies; where novel electrochemical bio affinity sensors were suggested for assessing the GEM and also to overcome the difficulties of the old fashion methods by easier availability, being more economical, reliable and non-invasive. However, a very important considerable matter was the interfering problem with other sort of treatments. This is indeed a drawback with this type of sensors despite of the benefits including good sensitivity and practical application. Therefore, there was an urgent need for improvement in this field by developing the biosensors with very low detection limits and high-selectivity in quantification of anti-cancer drugs.

Undoubtedly, molecularly imprinted polymers (MIPs) have been the center of attention between the scientists in analytical and bioanalytical chemistry in recent years. The MIPs were massively emphasized due to their specific identification sites for the template molecules, forming in the MIP tissue. Another benefit of MIPs was the great selectivity into the target templates. In fact, MIP performs as a template-polymer, synthesized by a solution which predominantly contains a monomer, target molecules as a template, and a cross-linker. The new selective bonds are formed between the cross-linked polymer and the template via reversible covalent or non-covalent interaction during the modified polymerization process. After the template removal step, the nano-sized cavities will still be remained; those are consistent with size, shape, and orientation of the template molecules. Therefore, the target molecule is determined when it is compared to the other species with similar structures.

Depending on the type of in-charged monomer during the MIP polymerization, various nanocomposites can be produced which can take a part in biosensors' structure. A good example is the siloxane-based materials, produced by the sol-gel method where the silane monomers are hydrolysed and condensed (Ribeiro et al., 2016; Olwill et al., 2004; Díaz-García. and Laíno, 2005). Biosensors modified by siloxane-based materials, display prominent chemical inertness, physical rigidity, and thermal stability. In the other words, molecular imprinting technique is associated to the sol gel process, known as molecularly imprinted siloxane (MIS). This phenomenon shows a promising and efficient alternative for fabricating electrochemical biosensing devices. It also offers excellent advantages such as high surface area and porosity, gelation, negligible swelling in organic solvents, and easy preparation at the room temperature; the latter is a critical issue when the weak interactions, with the target molecule, are concerned (Makote and Collinson, 1998a; Fireman- Shoresh et al., Makote and Collinson, 1998b, 2005; Farrington and Regan, 2009; Marx et al., 2004; Walcarius and Collinson, 2009; Sellergren, 2001). Also, it can be said, unlike the organic MIPs, imprinted siloxane polymer, as an inorganic molecularly imprinted polymer, shows higher specificity and capacity in an aqueous environment (Zaidi, 2016). Nevertheless, MIPs show astonishing properties which have made them a promising applicable tool in clinical analysis, medical diagnostics, environmental monitoring and drug delivery. Beside the MIPs strong points of stability, durability and reusability, their weak aspects are the lack of electrocatalytic activities and conductivities. Hence the MIPs modified biosensors usually have relatively low sensitivity (Lian et al., 2015; Haupt and Mosbach, 2000; Rezaei et al., 2015; Zaidi, 2013, 2014, 2017, 2018; Zaidi and Shin, 2014; Ziadi and Cheong, 2017).

In order to enhance the sensitivity and improve electrochemical responses of MIP films, several attempts and a range of materials, containing nanoparticles (NPs), were employed. The amendments to modify biosensors help to increase the electroactive surface area and electron transfer rate, and reduce the over-potential simultaneously (Rezaei et al., 2015; Zaidi, 2013, 2018; Zaidi and Shin, 2014; Shoja et al. 2016a, 2016b, 2017a, 2017b; Ghodsi et al., 2016a). Having introduced the nanomaterials and their potential effect on biosensors, the metallic NPs open up a new horizon in this field thanks to their exclusive optic properties, good conductivity, chemical stability and catalytic activity. These NPs have totally different properties and act in a different manner compare to their bulks. The metallic NPs have been widely used in optics, catalysis, and biosensing in the past decades (Bahadur et al., 2011; Filippo et al., 2013).

Silver (Ag) NPs, in particular, have been extensively employed in various fields e.g. catalysis, electronics, biosensors and so on. The remarkable advantages of Ag NPs are excellent stability, suitable biocompatibility, low toxicity and also they are rather more economical compare to other materials, (Filippo et al., 2013; Chen et al., 2014). A significant number of electrochemical sensors have been developed so far, by employing Ag NPs for detection of different analytes such as H_2O_2 (Li et al., 2013), glucose (Joshi et al., 2015), hydrazine (Zhao et al., 2015a,b), cholesterol (Li et al., 2010). Carbon nanotubes (CNTs) are also, one of the most common and effective modifiers which have been used to improve the efficiency of carbon paste electrodes (Ensafi and Karimi-Maleh, 2010; Beitollahi et al., 2012). CNTs are earning more credits in electrochemistry as a viable nanomaterial due to their extraordinary electronic properties, large surface area, significant mechanical strength, mass transfer capabilities, high catalytic capabilities and chemical and structural characteristics (Ghodsi et al., 2015; Cesarino et al., 2014).

Recently, DNA biosensors become favourite research topic because of their specific features. Probably one of the most interesting properties of DNA is their ability to bind small chemicals and biochemicals. This phenomenon leads to progress novel methods for recognizing many important molecules and biomolecules such as pathogens (Singh et al., 2013), drugs (Drevenšek et al., 2003; Lopes et al., 2013; Khan and Musarrat, 2013), and organic dyes (Guo and Dong, 2013; Vergani et al., 1997). In fact, interaction between DNA and small molecules occurs in two modes: covalent binding via chemical modifications of various DNA ingredient and reversible non-covalent binding mode by groove binding, electrostatic, and intercalation (Bartlett, 2008; Nowicka et al., 2007; Sirajuddin et al., 2013). Electrochemical evaluation of DNA and drug interactions have major applications according to their reliability as well as their rapid, and simple detections. Any interaction between chemical compounds and DNA is assessed and determined by investigating the DNA electrochemical properties. Direct monitoring of guanine and adenine oxidation states (Aydoğdu et al., 2016; Dogan-Topal and Ozkan, 2011) is taught to be an acceptable representative.

Eventually, after very careful investigations and detailed inspections, a novel electrochemical DNA biosensor was invented for selective assessment of GEM on the basis of molecularly bioimprinted technique. Ag NPs-based molecularly bioimprinted siloxane polymer (MBIS) was synthesized by using a sol-gel siloxane network in conjunction with ds-DNA. In fact, MIS and ds-DNA were utilized as dual recognition units.

GEM is likely to be the first line therapy of early and advanced stage

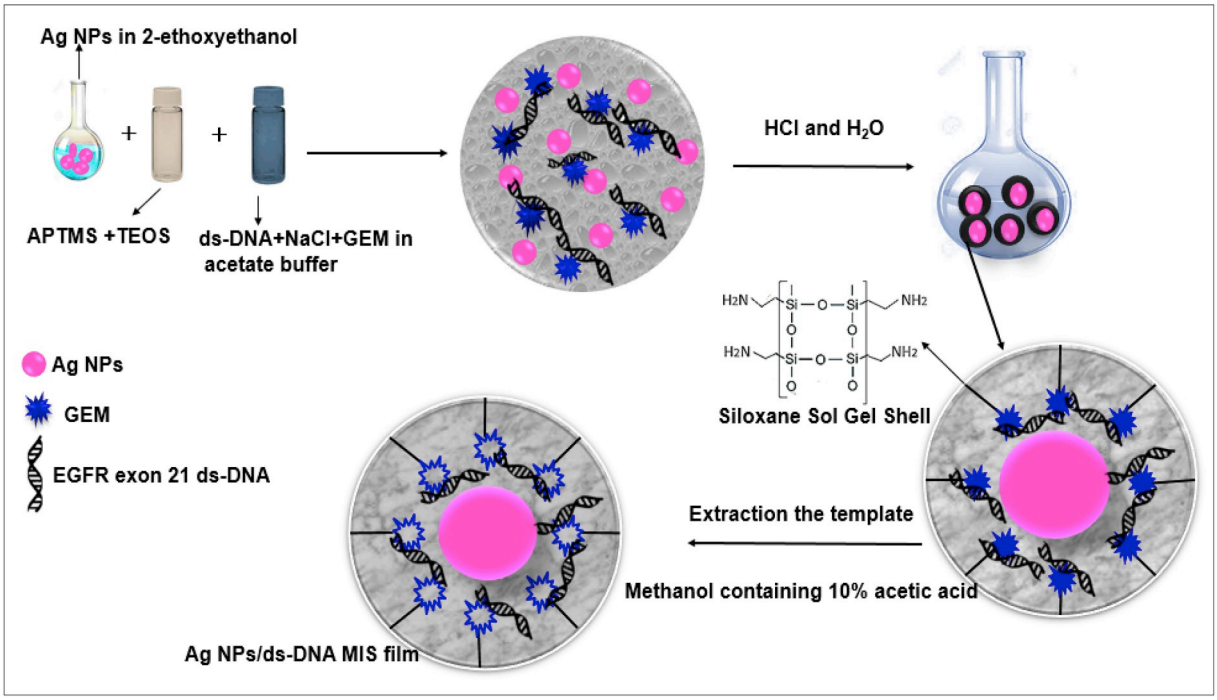

Scheme 2. All the synthesis steps of Ag NPs/ds-DNA MIS film.

non-small cell lung cancer (NSCLC). The treatment occurs by activating EGFR mutations, especially the L858R point mutation and exon 19 deletions. Therefore, EGFR exon 21 was selected with point mutation (L858R) and its complementary single-stranded DNA to form double helix structure (ds-DNA) as a bioreceptor for fabricating the biosensor. To the best of our knowledge, identifying GEM based on interaction with EGFR exon 21 has not been reported anywhere. In this work, a novel electrochemical nanobiosensor for detection and assessment of GEM was invented based on a new MBIS strategy in which the EGFR exon 21 acts as an identification probe.

2. Experimental procedures

2.1. Materials

The sample preparations were carried out employing the following ingredients: Tetraethoxysilane (TEOS), (3-amino propyl) trimethoxysilane (APTMS) and 2-ethoxyethanol (Merck, Germany); Ag NPs (average diameter of 30 nm) and MWCNTs (average diameter of 20–60 nm) (Neutrino Co., Iran); Gemcitabine (GEM) (Osveh Co., Iran). All oligonucleotides were synthesized and purified in specified labs of Takapouzist Co. (Tehran, Iran). Single-stranded DNA capture probe (ssDNA), for exon 21-point mutation (L858R), was 15- bases sequence: 5′ TTT GGC CCG CCC AAA3′. The sequence of 15-bases perfectly acts as a complementary target ss-DNA (ssDNAc) for ssDNA capture probe, shown as: 5′TTT GGG CGG GCC AAA3'. The made-up solutions were stored at 4 °C until use. All other reagents were of analytical grades. Acetate buffers were prepared from sodium acetate and acetic acid, pH values were adjusted by HCl and NaOH solutions. All acetate buffers, employed in the experiments, were in pH 4.8. The solutions were prepared using deionized water and deoxygenated by bubbling high purity (99.99%) nitrogen gas for 15 min prior to the experiments. All the experiments were carried out at room temperature.

2.2. Apparatus

Voltammetric measurements were performed using a three-electrode system, including the modified carbon paste electrode (CPE) as the working electrode, an Ag/AgCl (3.0 M KCl) as the reference electrode, and a platinum foil as the counter electrode. Voltammetric measurements were carried out using a computer-controlled μ-Autolab modular electrochemical system (PGSTAT101, Netherlands), driven with NOVA Software (V 1.10). All the electrochemical measurements in this work were performed by cyclic voltammetry (CV) and differential pulse voltammetry (DPV).

2.3. Synthesis of ds-DNA solution by hybridization with complementary target ssDNA

Hybridization process was considered to prepare the ssDNAc target. In this process two complementary strands of DNA formed a double-stranded molecule, which interacts with the ssDNA capture probe. This process was done by using 10 mL of 50 mM phosphate buffer solution (pH 7.0), containing the same specified optimum concentrations of ssDNA capture probe and ssDNA target for 60 min at 37 °C.

2.4. Synthesis of Ag NPs-based bioimprinted sol-gel film (Ag NPs/ds-DNA MIS)

Firstly, 15 mg of the Ag NPs was sonicated in 3 mL of 2-ethoxyethanol for 30 min (solution 1). Then a mixture solution, containing 130 μμL (0.74 mmol) of APTMS and 400 μL (1.8 mmol) of TEOS, was prepared (solution 2) and added to the solution 1 and stirred for 10 min (solution 3). Afterwards, 100 μL of an acetate buffer solution (pH 4.8, 0.5 M), containing 0.003 mg ds-DNA, NaCl, 0.02 M and 1.44 mg GEM, was prepared and added to solution 3 (solution 4). In order to obtain a homogeneous solution, 100 μL of 0.1 mol L^{-1} HCl and 90 μL of H_2O were added to the solution 4 and stirred for 2 h at the room temperature (Ribeiro et al., 2016; Rezaei et al., 2015). The obtained MIS coated Ag NPs NPs were centrifuged and washed with 2-ethoxyethanol at least three times to remove the excess dissolved TEOS and APTMS. Lastly, to obtain the Ag NPs/ds-DNA MIS film, the Ag NPs-based bioimprinted sol-gel film were immersed in a solution of methanol containing 10% acetic acid; the latter was to extract the template from the bioimprinted film and it took 30 min.

For the control check and further characterizations, the Ag NPs

(NBIS), coated by non-bioimprinted siloxane polymer/ds-DNA, and those coated by siloxane polymer (siloxane @ Ag NPs) were synthesized, for referencing purpose, by adding 100 µL of 0.1 mol L^{-1} HCl and 90 µL of H_2O to the solution 4 without GEM and solution 3 with respectively. The solutions were stirred for 2 h at the room temperature, to obtain a homogeneous sol. All the mentioned fabrication procedures are shown in Scheme 2.

2.5. Synthesis of the CPE/MWCNTs/Ag NPs/ds-DNA MIS

In order to fabricate a biosensor, applying optimized parameters according to our previous works (Ghodsi et al., 2015; Ghodsi et al., 2016b; Ghodsi et al., 2016c), a mixture of 10 mg Ag NPs/ds-DNA MIS film, 15 mg of MWCNTs, 75 mg of graphite and 80 µL of paraffin oil were prepared and completely mixed in a small oven. The obtained homogenous paste was packed into a tip of 1 ml insulin plastic syringe. A copper wire was attached to the pack for the external electric contact. Finally, the surface of the produced electrode (MBIS/CPE) was polished for further electrochemical tests. The non-bioimprinted siloxane polymer (NBIS)/CPE was produced with the similar procedure, but in absence of GEM, as a control biosensor. The fabrication process of CPE/MWCNTs/Ag NPs/ds-DNA MIS is shown in Scheme 3.

2.6. Electrochemical measurements

Cyclic voltammetry was employed to characterize the developed DNA biosensor for 1.0 mM $K_3Fe(CN)_6/K_4Fe(CN)_6$ (1:1) mixture containing 0.1 M KCl. Differential pulse voltammetry (DPV) was used for the detection of GEM via the change in electrochemical response of bases of DNA, like adenine and guanine pertain as a consequence of interacting with GEM. The DPV parameters were adjusted as follows: pulse amplitude 25 mV, pulse width 50 m s and scan rate 10 mVs^{-1}.

3. Results and discussion

3.1. Characterizations of Ag NPs/ds-DNA MIS film and CPE modified electrode

The morphology of the Ag NPs/ds-DNA MIS film was investigated by FE-SEM. The associated micrographs of Ag NPs, siloxane coated, and the ds-DNA MIS film coated Ag NPs are shown in Fig. 1a, b and 1c respectively. The average diameter of Ag NPs is about 30 nm in regular spherical shape (Fig. 1a). As it can be seen, the most of the NPs are relatively similar in size and shape; they all have smooth surfaces. Fig. 1b is related to the Ag NPs coated with siloxane. A core-shell nanostructure (siloxane @ Ag NPs) can clearly be distinguished. This is thought to be due to the presence of siloxane as a coating on the Ag NPs, which caused the increment in the average diameter of the NPs to about 60 nm. On the other hand, Fig. 1c shows the Ag NPs coated by ds-DNA MIS film with absolutely different topological shape and size; however, it is in total agreement with the work reported elsewhere (Dabrowski et al., 2018). In that case, it was thought that a nanostructured film was deposited on the surface of the NPs. The agglomeration of the NPs is also seen in the image as well as the increment of the diameter up to about 100 nm.

Figs. S1a, S1 b, S1c and S1d show the FE-SEM micrographs for MWCNT, CPE/MWCNT, and CPE/MWCNT/Ag NPs/ds-DNA MIS, respectively. Comparing Figs. S1a and S1b confirms that the diameter of the MWCNTs are increased which is due to the formation of CPE. Figs. S1c and S1d display CPE/MWCNT/Ag NPs/ds-DNA MIS at two different magnification; ds-DNA MIS coated Ag NPs are well dispersed in CPE/MWCNT matrix.

In the next step, FT-IR was employed to analyze the Ag NPs/ds-DNA MIS film. Fig. 2 shows the FT-IR spectra of Ag NPs (a), siloxane @ Ag NPs (b) and Ag NPs/ds-DNA MIS film (c). As it can be seen, the characteristic peak of Ag NPs can be observed at around 1639 cm^{--1} (Bahadur et al., 2011) in the spectrum (a); while in the other two

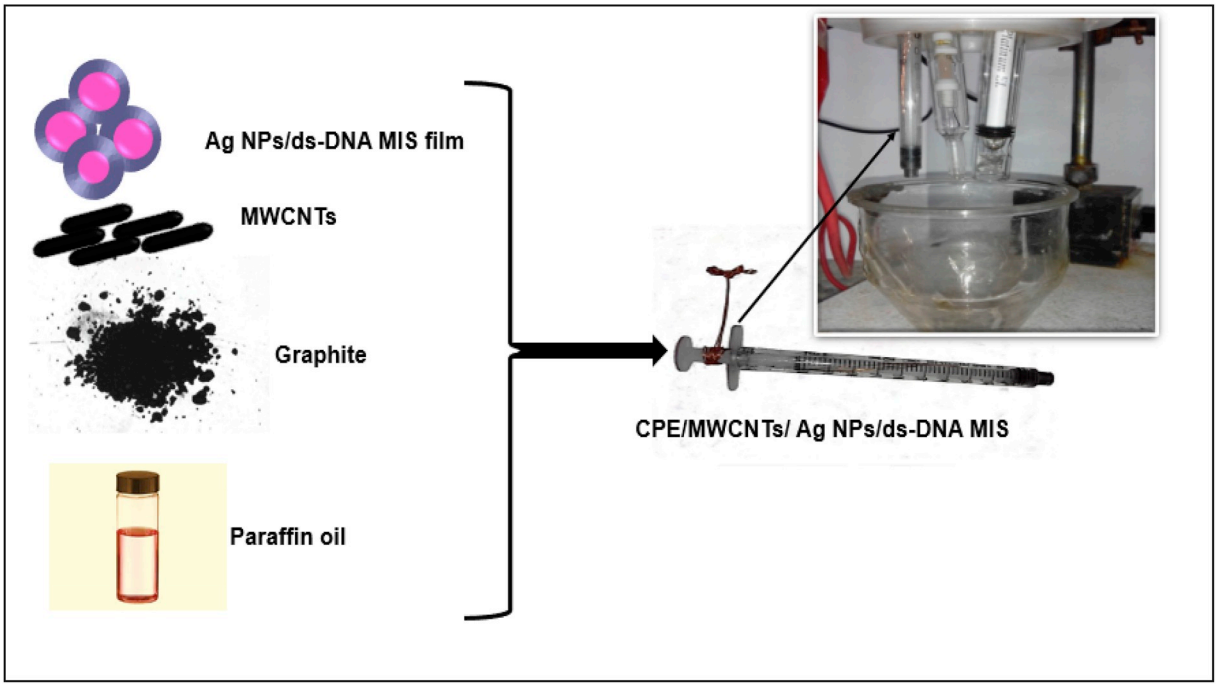

Scheme 3. Schematic fabrication of CPE/MWCNTs/Ag NPs/ds-DNA MIS.

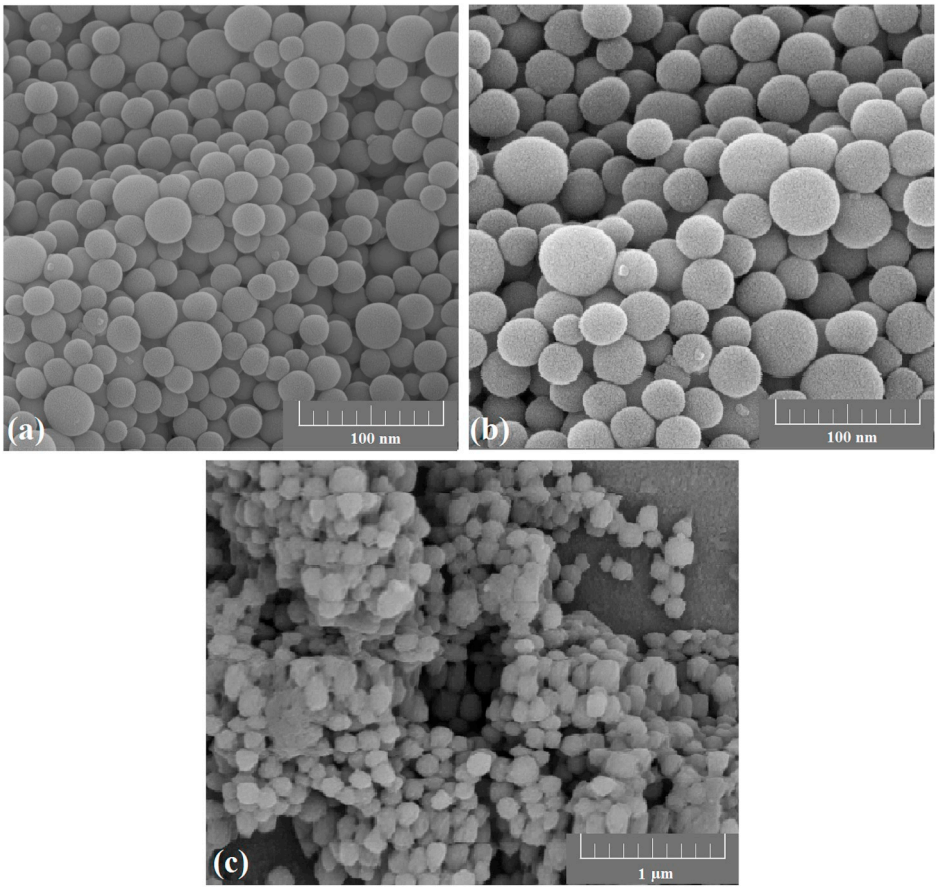

Fig. 1. FE-SEM images of (a) AgNPs, (b) siloxane @ Ag NPs and (c) ds-DNA MIS film coated Ag NPs.

spectra, (b) and (c), relatively strong absorption peaks are observed at 1097 cm^{--1}. The latter is assigned to the asymmetric stretching vibrations of the Si–O–Si from silica shells. Also peaks at around 469, 799 and 955 cm^{-1} are associated with the rocking vibrations of the Si–O–Si, bending vibrations of the Si–O–Si and bending vibrations of the SiO–H respectively. The peak widening phenomena are observed in area of around 3000 cm^{-1} (b and c), which are due to the SiO–H stretching vibrations (Dingemans et al., 2012).

Basically, there are three main regions known for DNA in FT-IR spectra. The first region indicates the asymmetric and symmetric PO^{2-} groups of the phosphodiester–deoxyribose backbone which can be seen from 950 to 1250 cm^{-1}. The second region is the signs of pyrimidine

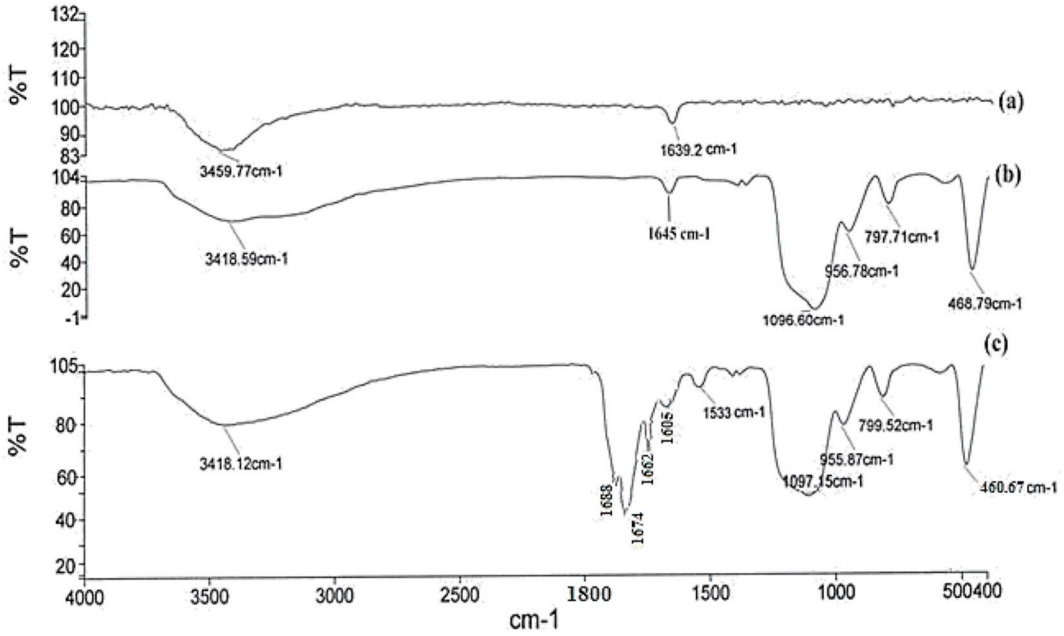

Fig. 2. FT-IR spectrums of (a) AgNPs, (b) siloxane @ Ag NPs, and (c) Ag NPs/ds-DNA MIS film.

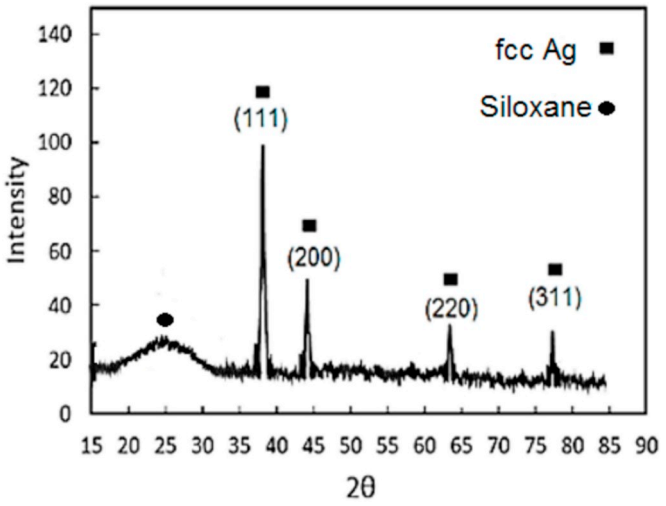

Fig. 3. XRD pattern of the siloxane @ Ag NPs.

and purine ring modes observed from 1500 to 1600 cm^{-1} and the third region is correlated to the C═O, C═N, C═C stretching and exocyclic $–NH_2$ bending vibrations in DNA bases. These areas are appeared from 1600 to 1750 cm^{-1}. In case of dsDNA, the assertion is on the amine bending and carbonyl stretching vibration bands since hydrogen bonds are greatly formed between the nitrogen of the amine group and oxygen of the carbonyl group. Two absorption bands found at 1688 cm^{-1} and 1605 cm^{-1} in spectrum (c), which are due to the presence of C═O and $–NH_2$ respectively (Wang and Son, 2013). The current peaks verified the presence of dsDNA on MIS shell coated on Ag NPs. Finally, the vibration band at 1674 cm^{-1} and 1662 cm^{-1} are assigned to the characteristic amine bending vibrations in GEM. Finally the bands appeared at 1533 cm^{-1} confirm the presence of amide band vibration in GEM (Khare et al., 2016; Draux et al., 2009).

The findings can clearly describe the important role of functional monomers in successful imprinting creation of siloxane film. The functional monomers are having support from deposited chemical functional groups inside the cavities. Condensation, stability, and rigidity process of the siloxane matrix around the template are obtained by TEOS and APTMS; where it contributes by a donor amine functional monomer capable of interacting with the GEM template via hydrogen bonding (Ribeiro et al., 2016).

The XRD pattern of siloxane @ Ag NPs is shown in Fig. 3. Diffraction peaks at around 38.2° (111), 44.2° (200), 64.7° (220) and 77.4° (311) are corresponding to the FCC structure of Ag NPs. These diffraction peaks are in absolute agreement with the Joint Committee on Powder Diffraction Standards cards (JCPDS) nos. 04–0783 (Zhao et al., 2015a,b). The presence of broadened peak over the range 2θ of 20° - 30° is related to the amorphous TEOS silica matrix. (Satvekar et al., 2012; Zhou et al., 2002).

EDS analysis was also carried out for MIS coated Ag NPs and Ag NPs/ds-DNA; the results are shown in Fig. 4a–b, respectively. Si peaks can be seen in both of 4a and 4b, corresponding to MIS shell on Ag NPs. The C and N peaks are associated with the DNA and siloxane film. The presence of P in Fig. 4a is particularly related to the ds-DNA probe that is entrapped on siloxane @ Ag NPs.

3.2. Electrochemical characterization of MWCNT/Ag NPs/MIS modified CPE

It is important for the active surface area to be measured prior to any electrochemical investigation. The active surface area can be defined as a microscopic characteristics of the modified electrodes; it was calculated employing the Randles–Sevcik equation and assuming concentration value of $K_4Fe(CN)_6$ as follows:

$$I_{pa} = 2.69 \times 10^5 n^{3/2} A D_R^{1/2} \nu^{1/2} C_0 \quad (1)$$

where I_{pa} is the anodic peak current, n the electron transfer number, A the surface area of the electrode, D_R the diffusion coefficient, C_0 the concentration of $K_4Fe(CN)_6$, and ν is the potential scan rate. The effective surface area can be extracted from the I_{pa}–$\nu^{1/2}$ plot by calculating the gradient of the curve for a known concentration of $K_4Fe(CN)_6$; where 1.0 mM $K_4Fe(CN)_6$ is in 0.10 M of KCl electrolyte with $n = 1$ and $D_R = 7.6 \times 10^{-6}$ cm s^{-1}.

Principally, the effective surface area and electron transfer rate, as two substantial electrochemical parameters of modified electrodes, are related to the peak height as well as the peak separation, respectively and can be calculated by equation (1). As mentioned previously, the effective surface areas of three electrodes (including developed MBIS biosensor and the others) were calculated by the gradient of the I_{pa}–$\nu^{1/2}$ curves (potential scan rate was 10–330 mV/S). They were 0.0154, 0.0619 and 0.33 mm^2 for CPE, CPE/MWCNT and CPE/MWCNT/Ag NPs/MIS respectively. Therefore, according the obtained results, the effective surface area for CPE/MWCNT is larger than that of CPE which perfectly highlights the role of MWCNT in term of improving the active surface area, comparing with the CPE. CPE/MWCNT/Ag NPs/MIS shows higher anodic and cathodic peak currents and consequently more effective surface area, compared to others. This can be related to the synergistic effect between MWCNT and Ag NPs and of course to presence of more active sites on the surface, where the electrooxidation reaction of $[Fe(CN)_6]^{3-}/[Fe(CN)_6]^{4-}$ takes a place.

CV voltammograms for 1.0 mM $K_4Fe(CN)_6$ in 0.10 M of KCl obtained by CPE, CPE/MWCNT and CPE/MWCNT/Ag NPs/MIS as work electrodes; the results are shown in Figs. S2a, S2b and S2c, respectively. Their corresponding I_{pa}–$\nu^{1/2}$ curves are also shown in Fig. 5. The linear graph confirms that the electrochemical activities are mainly controlled by diffusion during the oxidation of $K_4Fe(CN)_6$ at the surface. Finally, in order to realize the electrochemical characterization of MBIS biosensor, CV as an effective technique was applied for 1.0 mM $K_4Fe(CN)_6$ in 0.10 M of KCl for the sake of evaluating the obtained results at CPE, CPE/MWCNT, CPE/MWCNT/Ag NPs/MIS, and MBIS. The results (Fig. 6) showed that after formation of MBIS layer on Ag NPs, the peak current intensity of $[Fe(CN)_6]^{3-}/[Fe(CN)_6]^{4-}$ redox at MBIS biosensor surface was decreased apparently (curve d) comparing to CPE/MWCNT/Ag NPs/MIS (curve c). That can be described and related to the electrostatic repulsion between the negatively charged ds-DNA and $[Fe(CN)_6]^{3-}/[Fe(CN)_6]^{4-}$. On the other hand, the existence of imprinted cavities caused more improvement diffusion of $[Fe(CN)_6]^{3-/4-}$ through the MIS surface than CPE, CPE/MWCNT (curve a and b).

3.3. Electrochemical response of developed MBIS biosensor toward GEM sensing

The capability of the MBIS biosensor, to identify GEM on the sensing phase, was investigated by the electrochemical interaction between ds-DNA and GEM on the CPE/MWCNT/Ag NPs/ds-DNA MIS surface under optimal condition. Therefore, any change in oxidation signals of guanine and adenine was assumed as an indicator to evaluate the selective detection of GEM using DPV technique. The electrochemical oxidation of the residual guanine and adenine in ds-DNA, were monitored before and after interaction of ds-DNA with GEM on the surface of the invented biosensor. Fig. 7 illustrates different CPE responses (anodic peak currents in DPV measurement) in 0.5 M acetate buffer (pH 4.8) in absence and presence of 50 μM GEM. There were no anodic peak currents at the CPE/MWCNT and CPE/MWCNT/Ag NPs in absence and presence of GEM (a and b). Two well-defined anodic peaks were observed at around +1.0 and + 1.3 V, for CPE/MWCNT/Ag NPs/ds-DNA MIS film in absence and presence of GEM (c, d). They were associated with guanine and adenine oxidation respectively (Ensafi et al., 2012a, 2012b; Du et al., 2007). As shown in Fig. 7 (curve c), anodic signal currents for guanine and adenine in absence of GEM are higher than

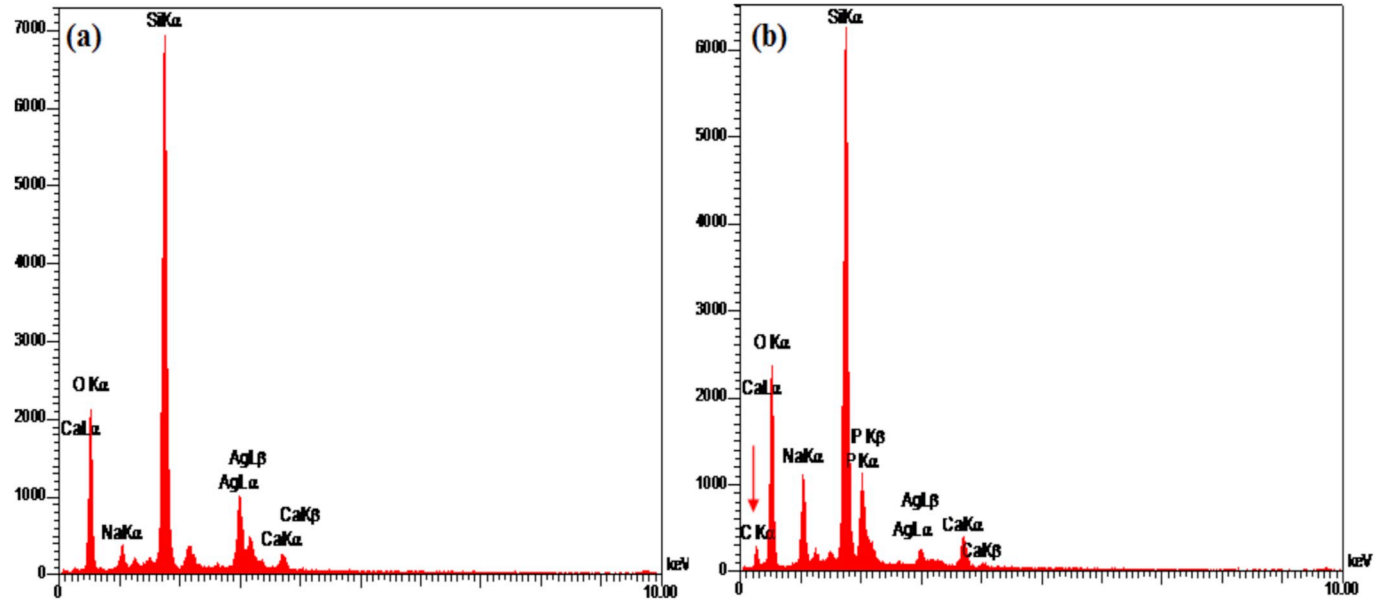

Fig. 4. EDX spectrum of (a) siloxane @ Ag NPs, and (b) Ag NPs/ds-DNA MIS film.

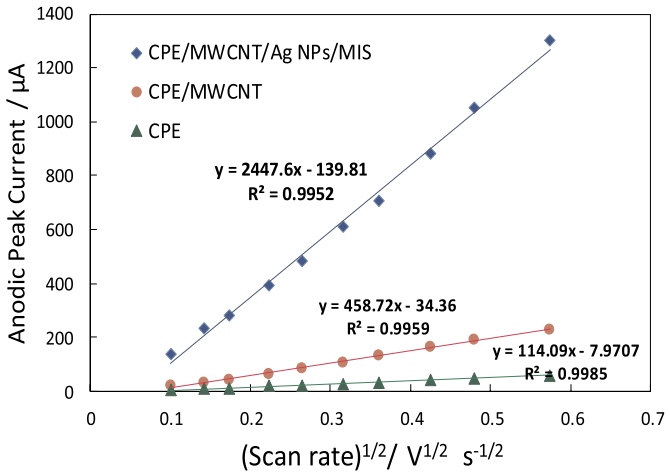

Fig. 5. The fitted I_{pa} (anodic peak current) versus the square root of the scan rates for CVs of CPE, CPE/MWCNT, and CPE/MWCNT/Ag NPs/MIS in 1 mM of $K_4Fe(CN)_6$ in 0.10 M of KCl.

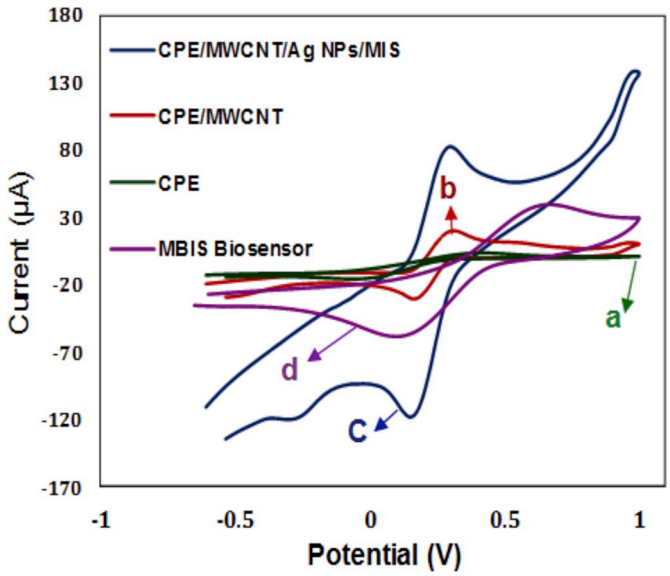

Fig. 6. CVs of (a) CPE, (b) CPE/MWCNT, (c) CPE/MWCNT/Ag NPs/MIS and (d) MBIS biosensor in 0.1M KCl solution containing 5.0 mM $K_3[Fe(CN)_6]$ at a scan rate of 100 mV/s.

those obtained in presence of GEM when the developed DNA biosensor is in charged (c).

In order to assess the electroactivity of GEM, a CPE/MWCNT was submerged in acetate buffer containing 50 µM GEM for 180 s in an open circuit. There was no significant oxidation peak of GEM at the CPE/MWCNT surface at the potential range between +0.40 and + 1.40 V. Hence, any change in oxidation peaks of the guanine and adenine were associated with their interaction with GEM; the residual amount in ds-DNA entrapped on the surface of the biosensor. Another important feature, which needs to be discussed in details, is the positive shifting of the oxidation peak potential of electroactive bases of ds-DNA; it can be seen clearly in Fig. 7d this phenomenon is due to the interaction of GEM with the guanine and adenine. In terms of electroactive bases of DNA, the negative or positive shifts occur due to the nature of bindings; whether they are electrostatic or intercalation interaction (Carter et al., 1989). Herein, the interaction mechanism between GEM and the ds-DNA is thought to be intercalative. Also, there is a possibility for the ds-DNA- GEM complex to be stabilized by hydrogen bonding and π–π stacking interactions. The last considerable aspect is the noticeable reduction and shifting anodic peak current of electroactive bases of entrapped ds-DNA at the Ag NPs-based MIS film. It can be described as a practicable damage while interacting with GEM; the results follow the Germ's therapeutic mechanism (Aydoğdu et al., 2016; Ensafi et al., 2012a). Considering all the experimental achievements and studying the obtained results, it seems to be convincing enough to state that by preparing MBIS, multi-functional groups were sit around the template target via cooperative interactions between the functional monomers and ds-DNA. In fact, siloxane film acts as an additional functional site by wrapping around ds-DNA and (Rezaei et al., 2015).

3.4. Optimizing the ds-DNA concentration and interaction time of GEM

The performance of the biosensors is directly related to the concentration of the entrapped ds-DNA and the interaction time. In Fig. S3 the adenine and guanine oxidation peak currents, obtained by DPV technique, are plotted as a function of ds-DNA concentration that

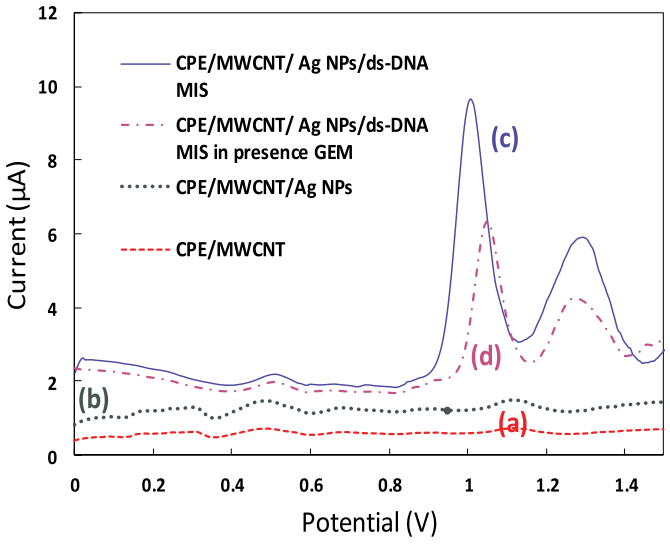

Fig. 7. DPV voltammograms of CPE/MWCNT (curve a), CPE/MWCNT/Ag NPs (curve b), CPE/MWCNT/Ag NPs/ds-DNA MIS film in absence GEM (curve c) and CPE/MWCNT/Ag NPs/ds-DNA MIS film in presence of GEM (curve d) in 0.5 M acetate buffer (pH 4.8).

participated in developed fabrication process. The optimized concentration was at the point of maximum oxidation signal currents from adenine and guanine. As it can be seen, electrochemical response of adenine and guanine has an increasing trend, when ds-DNA concentration increases from 5 mg L^{-1}–30 mg L^{-1}; after this point, the graph it slightly turns to plateau. Therefore, 30 mg L^{-1} was chosen as the optimum concentration. It is worth noting that, the steric effect followed by saturation of the electrode and repulsive electrostatics is potentially can be responsible for the obtained results (Shoja et al., 2018; Peterson et al., 2001).

In order to establish a valid protocol for the optimized conditions, a plan was defined as observation of guanine and adenine oxidation response currents while specific amount of GEM was added to the acetate buffer. In this case the oxidation peak current, related to the residual bases in ds-DNA, decreased to 180 s and then completely turned to plateau (Fig. S4), expressing the saturation of modified CPE/MWCNT with Ag NPs-based ds-DNA MIS film. Therefore, the following parameters were established to be the best operating parameters to be applied in this work; the concentration of ds-DNA to be 30 mg L^{-1} and an incubation time of 180 s.

3.5. Measurement and calibration curve at different concentrations of GEM

Having established the optimum conditions, the calibration curve was obtained by adding GEM to acetate buffer followed by DPV voltammograms. The results for a linear concentration range of 1.5–93 μM, are shown in Fig. 8a, the related calibration curves for GEM, according to changes in electrochemcial response of guanine and adenine, is also given in Fig. 8b. Also, the detection limit for this analyte was calculated to be 12.5 nmol L^{-1}, and 48.8 nmol L^{-1} via guanine and adenine successively. These linear concentration range and detection limits are absolutely acceptable in comparison with the other works reported previously. Table 1 gives an overview between our invented device compared to some other reported works in analytic point of views.

In case of the response time to the analyte, our developed biosensor remarkably achieved 95% of its maximum response to GEM in a competitive time, only 5s.

3.6. Effect of potential scan rate on the developed biosensor response

Having mentioned the satisfying achievements, in term of response

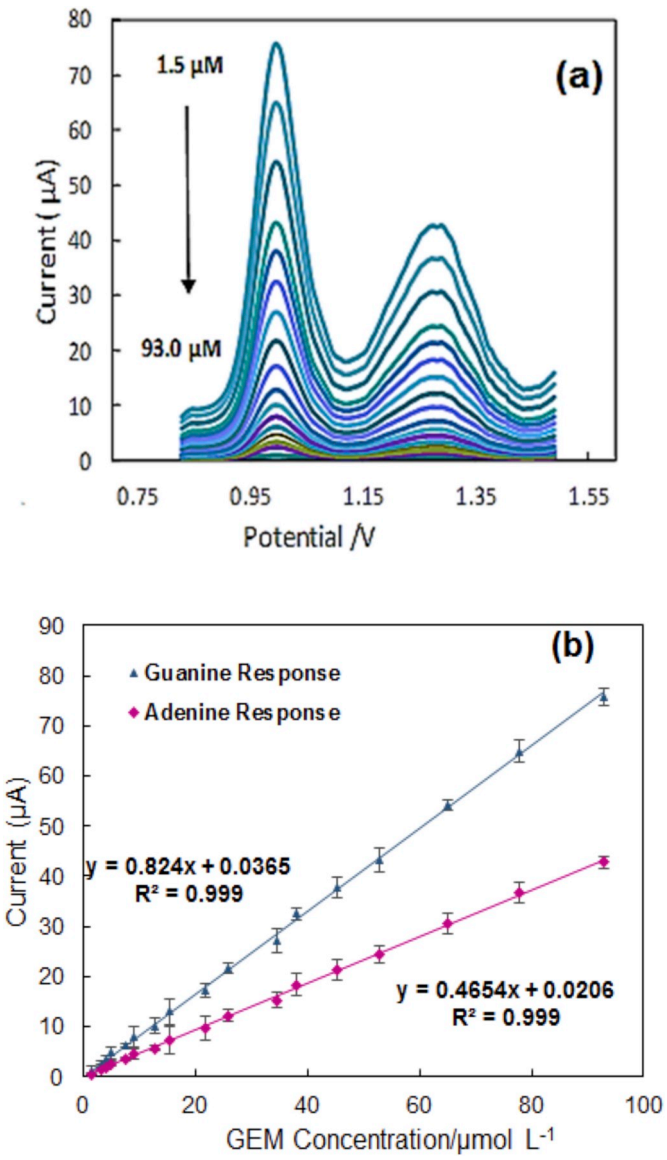

Fig. 8. (a) DPV voltammograms of CPE/MWCNT/Ag NPs/ds-DNA MIS in 0.5 M acetate buffer (pH 4.8) upon increasing the concentration of GEM in the range of 1.5 μM–93 μM under optimized condition, and (b) and its corresponding calibration curves for GEM based on the change of oxidation response of guanine and adenine.

time, the effect of the potential scan rate was also investigated. Fig. 9a shows the DPV voltammograms of 40 μmol L^{-1} of GEM in potential scan rate of 0.01–1.2 V/S. Anodic peak currents vs. square root of potential scan rate plots for guanine and adenine are shown in Fig. 9b. As it can be seen, the variables are in relation with a linear pattern; this indicates that diffusion is the dominant mechanism in kinetic of electrochemical processes during the analyte oxidation at the surface of the device.

3.7. Stability and reproducibility of the biosensor

As an important part of the development procedure, stability of the biosensor was also investigated. The stability test was carried out for 25 days at 4 °C; the results were reasonably promising. For the first 7 days, the electrochemical responses were constant in terms of adenine and guanine, however by reaching to the end of the period, the device maintained 65% of its maximum initial current response on the day one after fabrication. Reproducibility of the data was assessed by 4

Table 1
Comparison of developed MBIS biosensor performance in determination of GEM with other recently reported works.

Materials	Linear range	Detection limit	Reference
MIP/AuE	3.8 fmol L^{-1}_ to 38 nmol L^{-1}	3.0 fmL^{-1}	Florea et al., (2015)
GCE	5 μmol L^{-1} to 0.75 mmol L^{-1}	1.06 μmol L^{-1}	Kalanur et al.,(2009)
CPE	5.0_ × 10^{-8}–3.0 × 10^{-4} mol L^{-1}	8.2 × 10^{-9} mol L^{-1}	Teradal et al.,(2012)
AuE	0.1 — 15.0 μM L^{-1}	0.06 μM L^{-1}	Naik and Nandibewoor (2013)
GCE/P(PDCA)/dsDNA	3.8—114 μM L^{-1}	1.0 μM L^{-1}	Aydoğdu et al., (2016)
CPE/MWCNT/Ag NPs/ds-DNA MIS	1.5–93 μM	12.5 nmol L^{-1}	This work

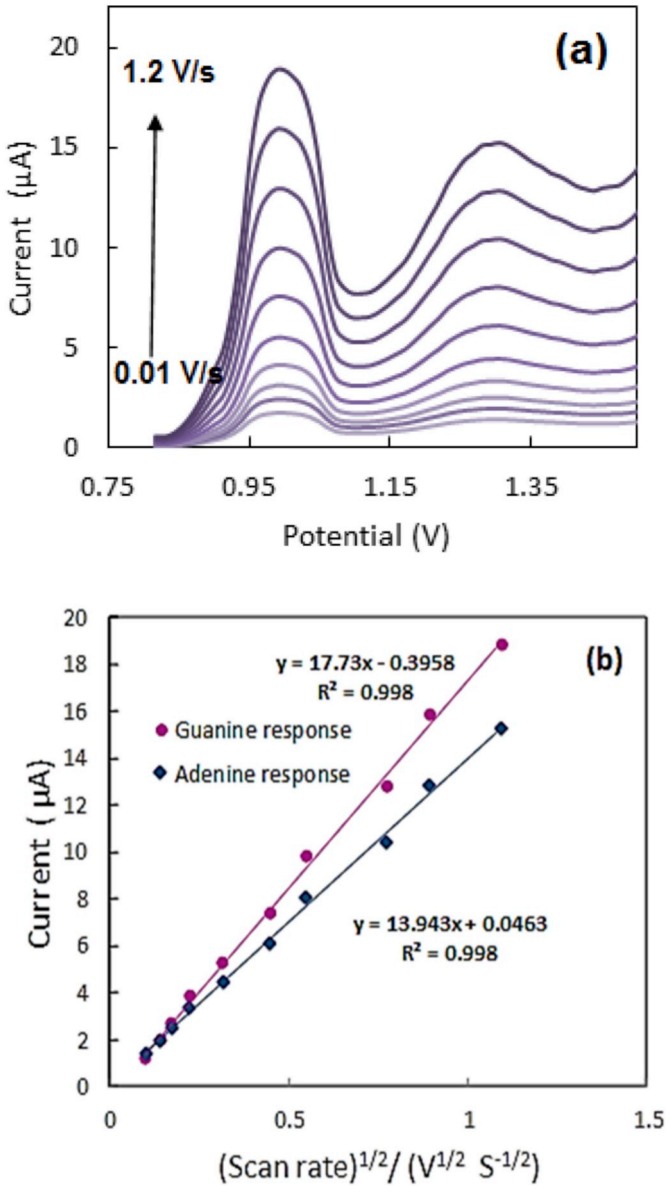

Fig. 9. (a) DPV voltammograms of CPE/MWCNT/Ag NPs/ds-DNA MIS in 0.5 M acetate buffer (pH 4.8) containing 40 μmol L^{-1} of GEM in potential scan rate of 0.01–1.2 V/s, and (b) obtained plots of anodic peak current vs. square root of potential scan rate for GEM based on the change of oxidation response of guanine and adenine.

successive measurement of constant concentration of GEM (40 μmol L^{-1}) by 4 different MBIS biosensor. Relative standard deviations were obtained (RSD) for adenine and guanine responses, which were 4.8% and 3.5% respectively.

Table 2
GEM determination in real sample.

Sample	Added (μM)	Expected (μM)	Found (μM)- The mean of three measured values	Recovery (%)
Serum	10.0	10.0	10.3	103.0
	15.0	15.0	14.6	97.4
	20.0	20.0	19.1	95.5

3.8. Selectivity and real sample analysis

Finally, applicability of the developed biosensor was examined with GEM determination in human serum as a real sample by standard addition method. The relevant results are summarized in Table 2. The relative recovery percentage (RR %) in Table 2 is determined by the following equation (Behbahani et al., 2014):

$$\text{Recovery (\%)} = (C_{found} - C_{real}/C_{added}) \times 100 \quad (2)$$

Where C_{added}, C_{found} and C_{real} are the concentrations of the specific amount of standard spiked to the real sample, the analyte after adding the specific amount of standard and the analyte in real sample, respectively. As it shown in Table 2, the recovery percentage, for GEM determination in serum sample, is 98.6% vs. guanine response which is totally acceptable for analyte determination. Indeed, the findings prove the applicability of our developed electrode in real samples.

The selectivity of MBIS CPE was examined by calculating the imprinting factor (IF) defined as the ratio of I_{MBIS} to I_{NBIS}. The IF of MBIS biosensor for GEM sensing with MBIS and siloxane @ Ag NPs CPE were found 6.5 and 4.1 with RSD of 3.1% and 3.9% respectively. Furthermore, in order to evaluation the interference compound effect on the response of modified biosensor, the electrochemical response of MBIS was investigated in human serum which naturally contains some relevant interference species such as ascorbic acid and uric acid at absence and presence of GEM. The results demonstrated the uric and ascorbic acid have no effect on the MBIS response for GEM detection since no changes were observed in oxidation peak current of guanine and adenine.

4. Conclusions

A novel and efficient electrochemical DNA biosensor has been introduced for GEM detection by employing MIS bio nanocomposite-based technique and ds-DNA EGFR exon 21-point mutant gene as both are a bioreceptor and electrochemical indicator. The characterizations proved that GEM molecules were successfully, imprinted onto the Ag NPs coated by siloxane polymer/ds-DNA; where Ag NPs were used as a signal amplifier. The specific sensing of GEM at a low concentration by MBIS biosensor, was done by interactions between GEM and EGFR exon 21 ds-DNA as well as the shape matching of imprinting cavities of the template. In terms of guanine and adenine, oxidation signals vary after GEM molecules interacted with functional groups in ds-DNA. Although, the developed CPE/MWCNTs/Ag NPs/ds-DNA MIS is capable of identifying GEM, its interaction with ds-DNA of EGFR exon 21-point mutant gene should be investigated carefully; it has an important role in designing anti-cancer drugs. It was proved that siloxane @ Ag NPs is

capable of acting as an easy and economical approach to synthesize electrodes for DNA immobilization, offering interesting electrocatalytic properties for electrochemical investigations. The current biosensor, when optimum conditions are applied, is a delicate measuring device providing suitable stability, wide linear range, short response time and low detection limit. Consequently, siloxane @ Ag NPs is strongly recommended for applying in other DNA and even enzymatic biosensors fabrication.

CRediT authorship contribution statement

Yalda Shoja: Conceptualization, Data curation, Formal analysis, Writing - original draft, Investigation, Methodology, Project administration. **Ahmad Kermanpur:** Supervision, Funding acquisition. **Fathallah Karimzadeh:** Supervision, Funding acquisition. **Javad Ghodsi:** Conceptualization, Data curation, Formal analysis, Writing - original draft, Investigation, Methodology, Project administration. **Amir Abbas Rafati:** Supervision, Funding acquisition. **Siavash Adhami:** Writing - review & editing.

Declaration of competing interest

The authors declare that they have no known competing financial interests or personal relationships that could have appeared to influence the work reported in this paper.

Acknowledgments

The authors greatly acknowledge Iran National Science Foundation (INSF, grant number: 95007216), Isfahan University of Technology (IUT) Research Council, Bu-Ali Sina University and Iran National Elites Foundation (INEF) for their financial support.

Appendix A. Supplementary data

Supplementary data to this article can be found online at https://doi.org/10.1016/j.bios.2019.111611.

References

Aydoğdu, G., Zeybek, T.B., Şule Pekyardımcı, S., 2016. Talanta 154, 312–321.
Bahadur, N.M., Furusawa, T., Sato, M., Kurayama, F., Siddiquey, I.A., Suzuki, N., 2011. J. Colloid Interface Sci. 355, 312–320.
Bartlett, P.N., 2008. John Wiley & Sons, Chichester, UK.
Behbahani, M., Najafi, F., Bagheri, S., Kalate Bojdi, M., Ghareh Hassanlou, P., Bagheri, A., 2014. Environ. Monit. Assess. 186, 2609–2618.
Beitollahi, H., Mohadesi, A., Mohammadi, S., Akbari, A., 2012. Electrochim. Acta 68, 220–226.
Carter, M.T., Rodriguez, M., Bard, A.J., 1989. J. Am. Chem. Soc. 111, 8901–8911.
Cesarino, V., Cesarino, I., Moraes, F.C., Machado, S.A., Mascaro, L.H., 2014. J. Braz. Chem. Soc. 25, 502–508.
Chen, S., Gao, H., Shen, W., Lu, C., Yuan, Q., 2014. Sens. Actuators B Chem. 190, 673–678.
Dabrowski, M., Lach, P., Cieplak, M., Kutner, W., 2018. Biosens. Bioelectron. 102, 17–26.
Díaz-García, M.E., Laíno, R.B., 2005. Microchim. Acta 149, 19–36.
Dingemans, G., Van Helvoirt, C., Pierreux, D., Keuning, W., Kessels, W., 2012. J. Electrochem. Soc. 159, H277–H285.
Dogan-Topal, B., Ozkan, S.A., 2011. Talanta 83, 780–788.
Drevenšek, P., Turel, I., Ulrih, N., 2003. J. Inorg. Biochem. 96, 407–415.
Draux, F., Jeannesson, P., Gobinet, C., Sule-Suso, J., Pijanka, J., Sandt, C., Paul Dumas, P., Manfait, M., Sockalingum, G.D., 2009. Anal. Bioanal. Chem. 395, 2293–2301.
Du, M., Xiaogang, H., Zihao, Z., Shouguo, W., 2007. Food Chem. 105, 883–888.
Ensafi, A.A., Heydari-Bafrooei, E., Amini, M., 2012b. Biosens. Bioelectron. 31, 376–381.
Ensafi, A.A., Karimi-Maleh, H., 2010. J. Electroanal. Chem. 640, 75–83.
Ensafi, A.A., Rezaei, B., Amini, M., Heydari-Bafrooei, E., 2012a. Talanta 88, 244–251.
Farrington, K., Regan, F., 2009. Talanta 78, 653–659.
Filippo, E., Manno, D., Buccolieri, A., Serra, A., 2013. Sens. Actuators B Chem. 178, 1–9.
Fireman-Shoresh, S., Turyan, I., Mandler, D., Avnir, D., Marx, S., 2005. Langmuir 21, 7842–7847.
Florea, A., Guo, Z., Cristea, C., Bessueille, F., Vocanson, F., Goutaland, F., Dzyadevych, S., Săndulescu, R., Jaffrezic-Renault, N., 2015. Talanta 138, 71–76.
Ghodsi, J., Rafati, A.A., Shoja, Y., 2016a. Sens. Actuators B Chem. 224, 692–699.
Ghodsi, J., Rafati, A.A., Shoja, Y., 2016b. Anal. Bioanal. Chem. 408, 3899–3909.
Ghodsi, J., Hajian, A., Rafati, A.A., Shoja, Y., Olena Yurchenko, O., Gerald Urban, G., 2016c. J. Electrochem. Soc. 163, B609–B616.
Ghodsi, J., Rafati, A.A., Shoja, Y., Najafi, M., 2015. J. Electrochem. Soc. 162, B69–B74.
Guo, Y., Dong, C., 2013. Electrochim. Acta 113, 69–76.
Haupt, K., Mosbach, K., 2000. Chem. Rev. 100, 2495–2504.
Honeywell, R., Laan, A.C., Groeningen, C.J., Strocchi, E., Ruiter, R., Giaccone, G., Peters, G.J., 2007. J. Chromatogr. B 847, 142–152.
Joshi, A.C., Markad, G.B., Haram, S.K., 2015. Electrochim. Acta 161, 108–114.
Kalanur, S.S., Katrahalli, U., Seetharamappa, J., 2009. J. Electroanal. Chem. 636, 93–100.
Khan, M.A., Musarrat, J., 2003. Int. J. Biol. Macromol. 33, 49–56.
Khare, V., Sakarchi, W.A., Gupta, P.N., Curtisa, A.D.M., Hoskins, C., 2016. RSC Adv. 6, 60126–60137.
Kirstein, M.N., Hassan, I., Guire, D.E., Weller, D.R., Dagit, J.W., Fisher, J.E., Remmel, R.P., 2006. J. Chromatogr. B 835, 136–142.
Lanz, C., Früh, M., Thormann, W., Cerny, T., Lauterburg, B.H., 2007. J. Sep. Sci. 30, 1811–1820.
Li, X., Liu, Y., Zheng, L., Dong, M., Xue, Z., Lu, X., Liu, X., 2013. Electrochim. Acta 113, 170–175.
Li, Y., Bai, H., Liu, Q., Bao, J., Han, M., Dai, Z., 2010. Biosens. Bioelectron. 25, 2356–2360.
Lian, W., Yu, X., Wang, L., Liu, H., 2015. J. Phys. Chem. C 119, 20003–20010.
Lopes, I.C., Oliveira, S.C., Oliveira-Brett, A., 2013. Anal. Bioanal. Chem. 405, 3783–3790.
Makote, R., Collinson, M.M., 1998a. Chem. Mater. 10, 2440–2445.
Makote, R., Collinson, M.M., 1998b. Chem. Commun. 3, 425–426.
Marx, S., Zaltsman, A., Turyan, I., Mandler, D., 2004. Anal. Chem. 76, 120–126.
Naik, K.M., Nandibewoor, S.T., 2013. J. Ind. Eng. Chem. 19, 1933–1938.
Nowicka, A.M., Zabost, E., Donten, M., Mazerska, Z., Stojek, Z., 2007. Anal. Bioanal. Chem. 389, 1931–1940.
Olwill, A., Hughes, H., O'Riordain, M., McLoughlin, P., 2004. Biosens. Bioelectron. 20, 1045–1050.
Peterson, A.W., Heaton, R.J., Georgiadis, R.M., 2001. Nucleic Acids Res. 29, 5163–5168.
Rezaei, B., Boroujeni, M.K., Ensafi, A.A., 2015. Biosens. Bioelectron. 66, 490–496.
Ribeiro, C.M., Miguel, E.M., Silva, J.S., DaSilva, C.B., Goulart, M.O.F., Kubota, L.T., Gonzaga, F.B., Santos, W.J.R., Lima, P.R., 2016. Talanta 156–157, 119–125.
Rosell, R., Crino, L., Danenberg, K., Scagliotti, G., Bepler, G., Taron, M., Alberola, V., Provencio, M., Camps, C., DeMarinis, F., Sanchez, J.J., Peñas, R., 2003. Semin. Oncol. 30, 19–25.
Satvekar, R.K., Phadatare, M.R., Karande, V.A., Patil, R.N., Tiwale, B.M., Pawar, S.H., 2012. Int. J. Basic Appl. Sci. 1, 468–476.
Sellergren, B., 2001. Elsevier, Amsterdam.
Shelley, M.D., Cleves, A., Wilt, T.J., Mason, M.D., 2011. BJU Int. 108, 168–179.
Shoja, Y., Kermanpur, A., Karimzadeh, F., 2018. Biosens. Bioelectron. 113, 108–115.
Shoja, Y., Rafati, A.A., Ghodsi, J., 2016a. Electrochim. Acta 203, 281–291.
Shoja, Y., Rafati, A.A., Ghodsi, J., 2017a. Mater. Sci. Eng. C 76, 637–645.
Shoja, Y., Rafati, A.A., Ghodsi, J., 2016b. Mater. Sci. Eng. C 58, 835–845.
Shoja, Y., Rafati, A.A., Ghodsi, J., 2017b. Enzym. Microb. Technol. 100, 20–27.
Singh, A., Sinsinbar, G., Choudhary, M., Kumar, V., Pasricha, R., Verma, H.N., Singh, S.P., Arora, K., 2013. Sens. Actuators B Chem. 185, 675–684.
Sirajuddin, M., Ali, S., Badshah, A., 2013. J. Photochem. Photobiol. B Biol. 124, 1–19.
Teradal, N.L., Kalanur, S.S., Prashanth, S.N., Seetharamappa, J., 2012. J. Appl. Electrochem. 42, 917–923.
Vergani, L., Mascetti, G., Gavazzo, P., Nicolini, C., 1997. Thermochim. Acta 294, 193–204.
Walcarius, A., Collinson, M.M., 2009. Annu. Rev. Anal. Chem. 2, 121–143.
Wang, X., Son, A., 2013. Environ. Sci.: Process. Impacts 15, 2204–2212.
Wickremsinhe, E.R., Lutzke, B.S., Jones, B.R., Schultz, G.A., Freeman, A.B., Pratt, S.E., Bones, A.M., Ackermann, B.L., 2010. Anal. Chem. 82, 6576–6583.
Zaidi, S.A., 2018. Sens. Actuators B Chem. 265, 488–497.
Zaidi, S.A., 2017. Biomater. Sci. 5, 388–402.
Zaidi, S.A., 2016. RSC Adv. 6, 88807–88819.
Zaidi, S.A., 2014. Drug Deliv. 23, 2262–2271.
Zaidi, S.A., Shin, J.H., 2014. Int. J. Electrochem. Sci. 9, 4598–4616.
Zaidi, S.A., 2013. Electrophoresis 34, 1375–1382.
Zaidi, S.A., Cheong, W.J., 2009. J. Chromatogr. A 1216, 2947–2952.
Zhao, J., Liu, J., Tricard, S., Wang, L., Liang, Y., Cao, L., Fang, J., Shen, W., 2015a. Electrochim. Acta 171, 121–127.
Zhao, K., Wu, C., Deng, Z., Guo, Y., Peng, B., 2015b. RSC Adv. 5, 52726–52736.
Zhou, Z.H., Xue, J.M., Wanga, J., Chan, H.S.O., Yu, T., Shen, Z.X., 2002. J. Appl. Phys. 91, 96015–96020.